Biogeosciences, 8, 3793–3808, 2011
www.biogeosciences.net/8/3793/2011/
doi:10.5194/bg-8-3793-2011

Biogeosciences

Particle-reactive radionuclides (^{234}Th, ^{210}Pb, ^{210}Po) as tracers for the estimation of export production in the South China Sea

C.-L. Wei[1], S.-Y. Lin[1], D. D.-D. Sheu[2], W.-C. Chou[3], M.-C. Yi[1], P. H. Santschi[4], and L.-S. Wen[1]

[1]Inst. of Oceanography, National Taiwan University, 23-13, Taipei 106, Taiwan
[2]Inst. of Marine Geology and Chemistry, National Sun Yat-sen University, Kaohsiung 804, Taiwan
[3]Inst. of Marine Environmental Chemistry and Ecology, National Taiwan Ocean University, Keelung 202, Taiwan
[4]Department of Oceanography and Marine Sciences, Texas A and M University, 200 Seawolf Parkway, Galveston, TX 77553, USA

Received: 15 September 2011 – Published in Biogeosciences Discuss.: 28 September 2011
Revised: 25 November 2011 – Accepted: 27 November 2011 – Published: 21 December 2011

Abstract. The time-series station, SEATS (18° N, 116° E) in the South China Sea was visited six times during October 2006–December 2008 to carry out seawater sampling and floating trap deployments for the determination of distributions and fluxes of POC, PIC, PN, ^{234}Th, ^{210}Pb, and ^{210}Po in the upper 200 m of the water column. Radionuclide deficiencies resulted in removal fluxes from the euphotic layer of 1.1×10^3–1.8×10^3 dpm m^{-2} d^{-1} and 7.1–40.2 dpm m^{-2} d^{-1} for ^{234}Th and ^{210}Po, respectively. Due to atmospheric input, an excess of ^{210}Pb relative to ^{226}Ra is commonly observed in the upper water column. Sinking fluxes of total mass, POC, PIC, PN, ^{234}Th, ^{210}Pb, and ^{210}Po measured at the euphotic depth were low in summer-fall and high in winter-spring, reflecting the seasonal variability of biological pumping. Excluding the suspiciously low primary productivity data point in July 2007, a relatively high e-ratio of 0.28–0.69 was estimated by the ratio of the POC flux at the euphotic depth and the integrated primary productivity. The ratios of ^{234}Th, ^{210}Pb, and ^{210}Po to organic carbon, inorganic carbon, and nitrogen in the sinking particles were combined with the disequilibria of ^{234}Th–^{238}U, ^{210}Pb–^{226}Ra, and ^{210}Po–^{210}Pb to estimate export fluxes of POC, PIC, and PN from the euphotic layer. Compared with measured fluxes by the sediment trap and estimated fluxes by other approaches, it is concluded that the export production in the South China Sea, ranging from 1.8 to 21.3 mmol-C m^{-2} d^{-1}, can be reasonably estimated using ^{234}Th, ^{210}Pb, and ^{210}Po as carbon proxies.

Correspondence to: C.-L. Wei
(weic@ntu.edu.tw)

1 Introduction

It is known that carbon dioxide sequestration from the atmosphere in the ocean depends, in part, on the magnitude of carbon removal via particle settling from the surface to the deep layer of the ocean. Thus, the quantification of export flux from the euphotic zone is of great importance to the understanding of carbon cycling in the ocean. The SEATS site, a time-series station regularly visited by Taiwanese oceanographers since 1999, is located at 18° N 116° E in the central basin of the South China Sea (Wong et al., 2007). Although being in a marginal sea, the site shows open-ocean characteristics with low productivity. The SEATS is an ecosystem dominated by picoplankton with a relatively low primary productivity ranging between 300 mg-C m^{-2} d^{-1} in summer to 550 mg-C m^{-2} d^{-1} in winter (Chen et al., 2004; Chen and Chen, 2005). The South China Sea has a thin surface mixed layer of 30–80 m and a constant euphotic depth of 100 m, which make the diffusive flux of nutrients an important mechanism of supporting the primary production in this oligotrophic system (Tseng et al., 2005).

Despite the fact that previous estimates of the export flux of particulate organic carbon (POC) at the SEATS in the South China Sea were attempted by various approaches, e.g. biochemical modeling (Liu et al., 2002), carbon budgeting (Chou et al., 2006), and new productivity measurements (Chen and Chen, 2005; Chen et al., 2004), the magnitude of POC export from the euphotic zone has never directly been measured. Previously, short-lived particle-reactive radionuclides, ^{234}Th ($t_{1/2}$ =24.1 d), ^{210}Pb ($t_{1/2}$ = 22.4 a), and ^{210}Po ($t_{1/2}$ = 138 d), have been found to be very useful for the estimation of export production in the ocean. Among the three,

^{234}Th has been widely used as a powerful tracer for POC and provided estimates of the export production (see review of Buesseler, 1998). There is only a few studies that used ^{210}Pb to estimate the export production in the ocean, although a strong correlation of ^{210}Pb removal with the POC flux was previously demonstrated (Moore and Dymond, 1988). On the other hand, due to its high affinity with biological particles (Cherry et al., 1975), ^{210}Po is also used as a powerful tracer for particulate matter sinking out of surface ocean (Murray et al., 2005; Friedrich and Rutgers van der Loeff, 2002; Verdeny et al., 2009; Kim and Church, 2001; Buesseler et al., 2008).

Here we report the results of POC, PIC, and PN export fluxes directly measured by floating traps deployed in six cruises to the SEATS during October 2006–December 2008. The export fluxes were also estimated from the distributions of the three particle-reactive radionuclides in the euphotic layer. The goals of this study therefore are Eq. (1) to investigate the temporal variability of particle scavenging and removal processes, Eq. (2) to compare the geochemical behavior of ^{234}Th, ^{210}Pb, and ^{210}Po, and Eq. (3) to estimate the export flux of POC, PIC, and PN by ^{234}Th/^{238}U, ^{210}Po/^{210}Pb, and ^{210}Pb/^{226}Ra disequilibria in the euphotic layer of the northern South China Sea.

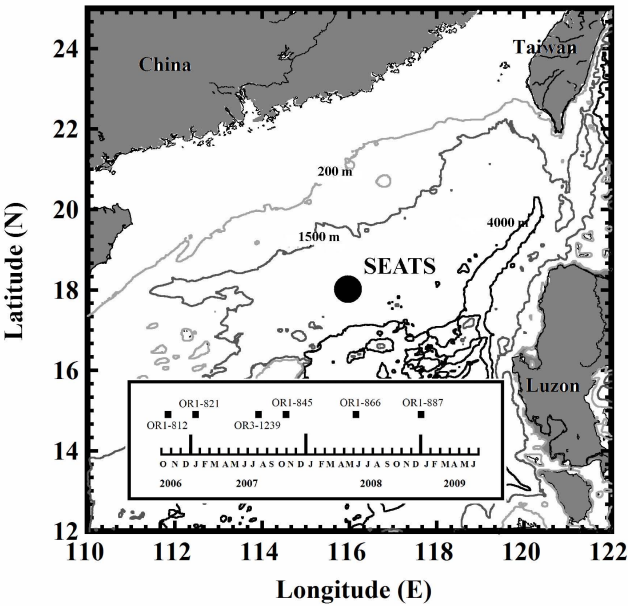

Fig. 1. Location of SEATS station in the South China Sea. Inserted box shows the timeline of the six cruises to the station.

2 Material and methods

Seawater samples were collected by multiple cruises to the SEATS site in the South China Sea on board the R/V *Ocean Researcher I or III* (refer to Fig. 1 for the timeline of the cruises).

2.1 Seawater

Seawater was collected using either 10 l (R/V *Ocean Researcher III*) or 20 l (R/V *Ocean Researcher I*) Teflon-coated Go-Flo bottles mounted on a Sea-Bird® CTD (SBE 9/11) rosette system. Except for the first cruise (ORI-812), from which only ^{234}Th activity in unfiltered seawater was measured, filtration of large-volume seawater for the determination of ^{234}Th, ^{210}Pb, and ^{210}Po activities in filtrate and particles was carried out for all samples. At each sampling depth, 40 l seawater was collected and divided into one 20 l and two 10 l subsamples. The 20 l sample was used to determine ^{234}Th and the two 10 l samples were used to determine ^{210}Pb and ^{210}Po, respectively. Seawater was immediately pressure-filtered by compressed air through a pre-weighed 142 mm Nuclepore filter (0.45 µm) mounted in a Plexiglas filter holder. Filtrate and particles retained on the filter were processed and analyzed for ^{234}Th, ^{210}Pb, and ^{210}Po activities following the procedures described in Wei et al. (2009).

In short, approximately 20 ml of concentrated HCl along with 35 dpm ^{230}Th yield tracer as well as 60 mg Fe carrier was added into the 20 l filtrate sample. Given at least 10 h for isotopic equilibration, 12 N NaOH was added to raise the pH to 8 to form $Fe(OH)_3$ precipitate. The $Fe(OH)_3$ precipitate was collected by siphoning and centrifuging, and then dissolved in concentrated HCl to make the samples 9 N HCl. These samples were then passed through an anion exchange column (AG1X-8) preconditioned by 9 N HCl to separate uranium from thorium. Thorium samples were purified by passing the sample through three anion exchange columns pre-conditioned with 8 N HNO_3. The sample was evaporated down to one drop and was ready for extraction. ^{234}Th and the yield tracer, ^{230}Th, were extracted into a 0.4 M TTA (thenoyltrifluoroacetone)-benzene solution and stippled on a stainless-steel disc. Preconcentration and separation of uranium and thorium from the filtered seawater samples were completed in five days after samples were collected.

The particulate samples collected on the Nuclepore filters were dried in a desiccator and weighed to estimate the concentration of total suspended matter. After adding 10 dpm ^{230}Th yield tracer, the filter was decomposed and digested by HNO_3/HCl/$HClO_4$/HF. The samples were purified and mounted on stainless-steel discs following the same procedures as for dissolved ^{234}Th samples. The activities of ^{234}Th were counted by a low background (<0.15 cpm) anticoincidence counter (Riso GM25-5) via its β-emitting daughter ^{234}Pa. Chemical yield of thorium was estimated by counting spiked ^{230}Th using silicon surface-barrier detectors (EG&G Ortec 576).

The filtrate from the 10 l sample for ^{210}Po determination was acidified with about 10 ml concentrated HCl and spiked with 2.2 dpm of ^{209}Po and 30 mg of Fe carrier. Given 2 days isotopic equilibration time, concentrated NH_4OH

was then added to raise the pH∼8 to precipitate $Fe(OH)_3$. The $Fe(OH)_3$ precipitate was collected by decanting and centrifuging and dissolved in HCl, digested with HNO_3, and ^{210}Po and ^{209}Po were spontaneously plated onto silver plates. The particulate samples collected on the Nuclepore filters were dried in a desiccator and weighed to estimate the concentration of total suspended matter. After adding 2.2 dpm of ^{209}Po, the filter was decomposed and digested by HNO_3/HCl/$HClO_4$/HF. ^{210}Po and ^{209}Po were plated onto silver plates following the same procedures as for dissolved samples. The 10 l seawater samples for ^{210}Pb determination were stored for at least 1 yr to let ^{210}Po grow in from ^{210}Pb; then the same procedures for dissolved and particulate ^{210}Po were followed. The silver discs were counted by alpha spectrometry (EG&G Ortec 576). All activities of ^{234}Th and ^{210}Po reported here were corrected back to the sampling time after the ingrowths from parent radionuclides were subtracted.

Auxiliary standard oceanographic variables (e.g. nutrients, primary productivity, etc.) were measured by technical personnel of SEATS program. Nutrients were determined following the methods of Strickland and Parsons (1984). Primary productivity was determined by $Na^{14}HCO_3$ incubation of seawater samples collected from 6–8 depths in the upper 100 m.

2.2 Floating trap

Particle interceptor trap (Wei et al., 1994) was deployed for the measurement of vertical fluxes of total mass (F_{Mass}), ^{234}Th (F_{Th}), ^{210}Po (F_{Po}), ^{210}Pb (F_{Pb}), particulate carbon (F_{PC}), particulate nitrogen (F_{PN}), and particulate organic carbon (F_{POC}), at three depths (30 m, 100 m, 160 m). At each depth, a set of sediment traps consisting of eight Plexiglas tubes filled with trap solution prepared from the mixture of filtered seawater and formaldehyde (0.3 % v/v) were snapped on a polypropylene cross frame, which is secured to a mooring line. It should be noted that radionuclide release into overlying waters in unpoisoned traps (even when deployed for less than 1 day) has been documented (Hung et al., 2010; Xu et al., 2011), which can underestimate radionuclide fluxes. The mooring array was left free drifting for 37–48 h. Upon recovery, the upper layer of seawater in the tube was siphoned off and the remaining trap solution was filtered through a pre-weighed 90 mm Nuclepore filter (0.45 µm pore size). The swimmers, mainly macrozooplanktons, were picked under a microscope. The samples then were rinsed by deionized water to remove salts. The filters were then dried in a desiccator and weighed for total mass flux calculation. The filters were analyzed for ^{234}Th, ^{210}Pb, and ^{210}Po activities following the procedures as particulate samples described in previous section.

The samples in tubes used for carbon and nitrogen analyses were filtered through pre-combusted Whatman 25 mm GF/F filters. After swimmers were picked, the filters were wrapped firmly into tin boats and loaded into the autosampler of EA elemental analyzer (EuroEA3000) for total carbon and nitrogen content. The filters for organic carbon analysis were fumed for 24 h with concentrated HCl to remove calcium carbonate, then analyzed for carbon content. Fluxes of particulate inorganic carbon (F_{PIC}) were calculated by difference of F_{PC} and F_{POC}. The overall procedural error are better than ±2 % for both carbon and nitrogen determinations.

3 Results

3.1 ^{234}Th, ^{210}Pb, and ^{210}Po in seawater

Vertical profiles of ^{234}Th activity concentrations of dissolved ($^{234}Th_d$) and particulate ($^{234}Th_p$) in the upper 20 m at SEATS station, as well as TSM concentrations, are shown in Fig 2. It should be noted that only total ^{234}Th ($^{234}Th_t$) concentrations are available for October 2006 (ORI-812). Except for the subsurface layer in October 2007, the $^{234}Th_d$ values are significantly lower than those of ^{238}U, indicating active scavenging in the upper water column. The $^{234}Th_p$ values fall in the range from 0.05 to 0.75 dpm l^{-1} and sometimes show similar vertical distributions as TSM (Fig. 2). Vertical profiles of ^{210}Pb activity concentrations of dissolved ($^{210}Pb_d$) and particulate ($^{210}Pb_p$) in the upper 200 m at SEATS station, and TSM concentrations from the filtration of ^{210}Pb samples are shown in Fig. 3. The line showing vertical distribution of ^{226}Ra was estimated from SiO_2 concentration by ^{226}Ra (dpm 100 l^{-1}) = 5.15 + 0.14 SiO_2 (µmol $^{-1}$), which is based on the data determined at the site 300 km to the south of the SEATS by Nozaki and Yamamoto (2001). An excess of ^{210}Pb relative to ^{226}Ra in the upper water column is generally found. The $^{210}Pb_p$ concentrations are much lower than the $^{210}Pb_d$ concentrations, and show no systematic variation with depth. Vertical profiles of ^{210}Po activity concentrations of dissolved ($^{210}Po_d$) and particulate ($^{210}Po_p$ in the upper 200 m at SEATS station, and TSM concentrations from the filtration of the ^{210}Po samples are shown in Fig. 4).

3.2 Sinking fluxes

Sinking fluxes of total particulate matter or mass (F_{Mass}), POC (F_{POC}), PIC (F_{PIC}), PN (F_{PN}), ^{234}Th (F_{Th}), ^{210}Pb (F_{Pb}), and ^{210}Po (F_{Po}) at the three deployment depths (30, 100, and 160 m) are shown in Fig. 5a–g, respectively. The average, range, and standard deviation of sinking fluxes of various parameters are summarized in Table 1. In general, all fluxes decreased with depth. Although the fluxes for all components, except ^{210}Pb, show the largest variability with a RSD of >70 % at 30 m, the correlations between fluxes are noticeably high, with correlation coefficients of >0.9 between all combinations of flux parameters. Except for the F_{PIC}, and F_{Po}, all fluxes varied within a relatively small range, with a RSD of ∼40 % at 100 m, the approximate euphotic depth at SEATS.

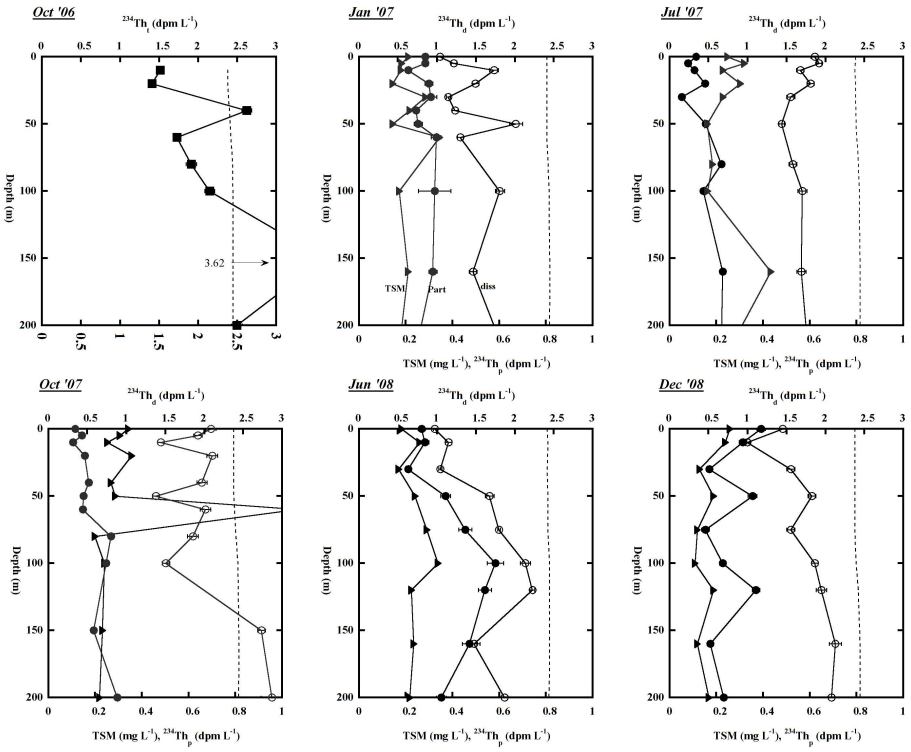

Fig. 2. Vertical distributions of dissolved (open circle) and particulate (solid circle) ^{234}Th, TSM concentration (solid triangle), and the ^{238}U (thick dotted line) calculated from salinity (Ku et al., 1977). Note only total ^{234}Th (solid square) is available for ORI-821 (October 2006). Error bars represent uncertainty based on propagated counting errors ($\pm 1\sigma$).

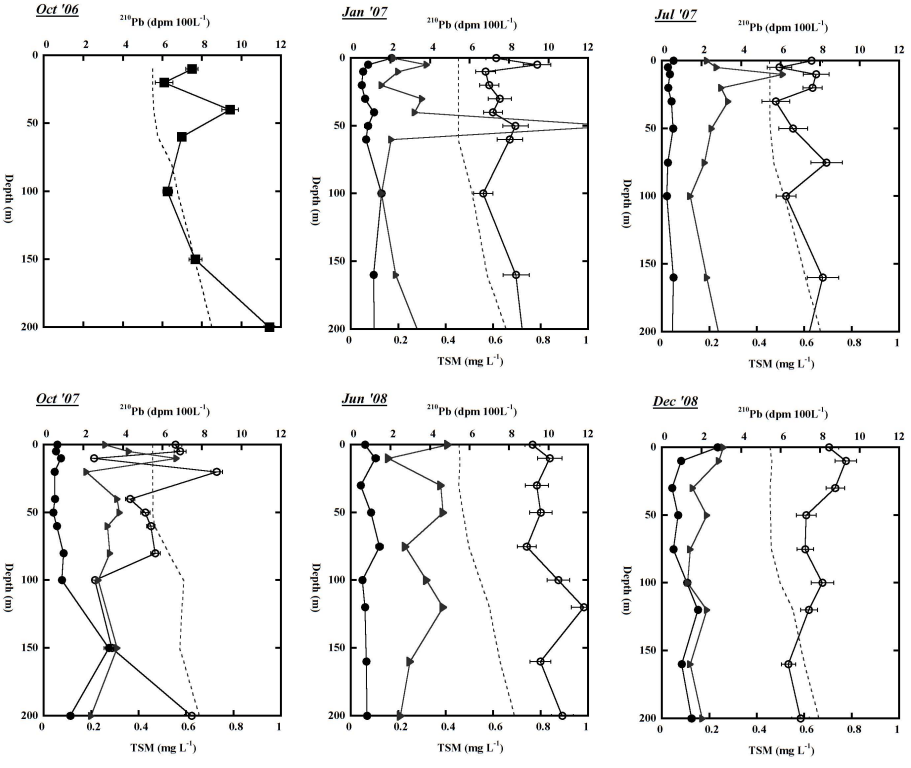

Fig. 3. Vertical distributions of dissolved (open square) and particulate (solid square) ^{210}Pb, TSM concentration (solid circle), and the ^{226}Ra (thick dotted line) estimated from SiO_2 (Nozaki and Yamamoto, 2001). Note only total ^{210}Pb (solid triangle) is available for ORI-821 (October 2006). Error bars represent uncertainty based on propagated counting errors ($\pm 1\sigma$).

Table 1. Range, average, and standard deviation of sinking fluxes of total mass (F_{Mass}), POC (F_{POC}), PIC (F_{PIC}), PN (F_{PN}), ^{234}Th (F_{Th}), ^{210}Pb (F_{Pb}), and ^{210}Po (F_{Po}) at three depths during October 2006 and December 2008.

Depth m	F_{Mass} mg m^{-2} d^{-1}	F_{POC}	F_{PIC} mmol m^{-2} d^{-1}	F_{PN}	F_{Th}	F_{Pb} dpm m^{-2} d^{-1}	F_{Po}
30	441 ∼ 3548 1776 ± 1249	8.6 ∼ 59.1 29.6 ± 19.0	3.7 ∼ 23.8 11.8 ± 9.1	2.7 ∼ 10.1 6.0 ± 3.1	694 ∼ 3395 1778 ± 1187	17.4 ∼ 36.4 27.6 ± 7.8	33.6 ∼ 127.4 72.3 ± 45.5
100	597 ∼ 1215 861 ± 256	9.8 ∼ 18.5 14.4 ± 3.3	2.1 ∼ 9.5 5.2 ± 3.1	1.5 ∼ 4.1 2.4 ± 0.9	1201 ∼ 2160 1690 ± 399	7.5 ∼ 33.8 23.0 ± 9.6	10.6 ∼ 107.6 49.2 ± 39.4
160	285 ∼ 1095 638 ± 309	3.2 ∼ 10.8 6.9 ± 2.8	0.4 ∼ 8.3 2.6 ± 3.2	0.5 ∼ 1.7 0.9 ± 0.5	1046 ∼ 1864 1432 ± 304	14.0 ∼ 37.0 23.1 ± 10.7	11.5 ∼ 42.4 30.2 ± 15.2

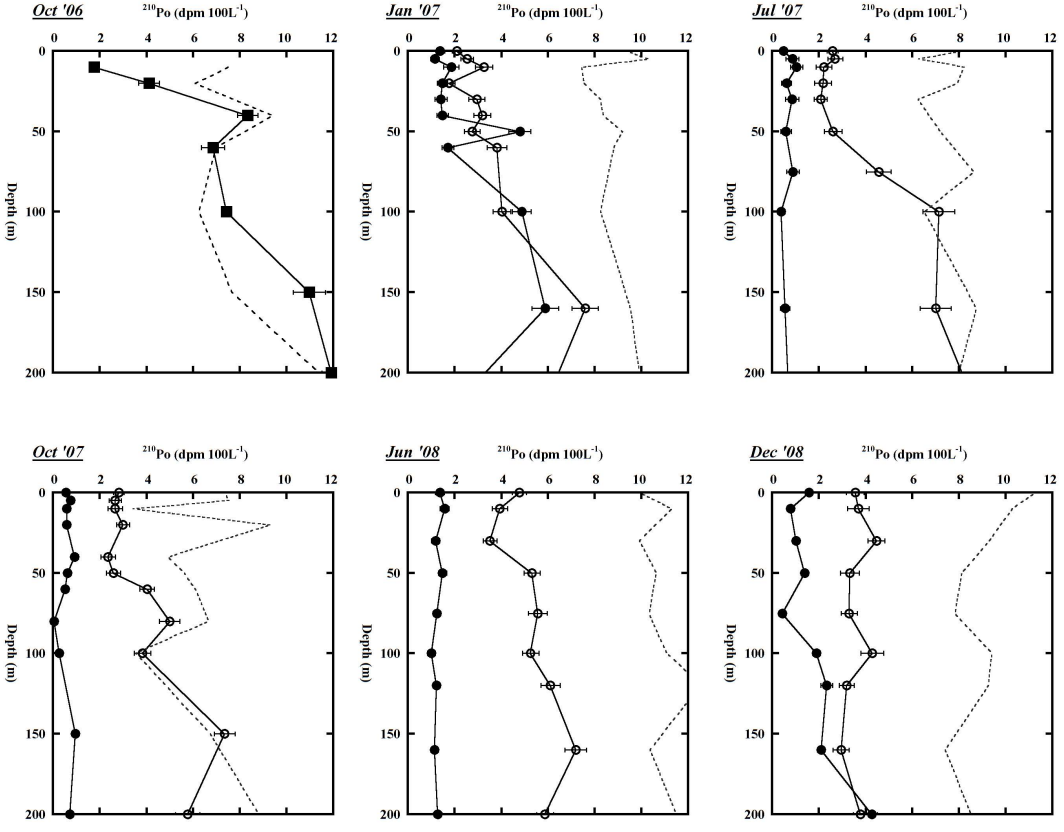

Fig. 4. Vertical distributions of dissolved (open square) and particulate (solid square) ^{210}Po, TSM concentration (solid circle), and total ^{210}Pb (thick dotted line) calculated by the sum of ^{210}Pb$_d$ and ^{210}Pb$_p$. Note only total ^{210}Po (solid triangle) is available for ORI-821 (October 2006). Error bars represent uncertainty based on propagated counting errors ($\pm 1\sigma$).

4 Discussions

4.1 Deficiencies and fluxes of ^{234}Th, ^{210}Po, and ^{210}Pb

There are very few previous open ocean studies that report ^{234}Th, ^{210}Pb, and ^{210}Po data determined from the same site. Among those few, Sarin et al. (1994) reported three vertical profiles of dissolved activity concentrations of ^{234}Th, ^{210}Pb, and ^{210}Po in the northeastern Arabian Sea. Wei and Murray (1991, 1994) compared the geochemical behavior of ^{234}Th, ^{210}Pb, and ^{210}Po in the Black Sea. Shimmield et al. (1995) measured the three radionuclides from the same seawater samples collected in the upper 500 m from the marginal ice zone in the Antarctica. Kim and Church (2001) presented dissolved and particulate ^{234}Th, ^{210}Pb, and ^{210}Po data determined on the same samples collected from the

Sargasso Sea. Murray et al. (2005) reported a complete ^{234}Th, ^{210}Pb, and ^{210}Po data set measured from seawater samples and settling particles collected by floating traps deployed in the Equatorial Pacific.

Vertical profiles showing the nuclide ratios of ^{234}Th and ^{238}U, ^{210}Po and ^{210}Pb, and ^{210}Pb and ^{226}Ra in the upper 200 m obtained from the six cruises are given in Fig. 6. Relative to their parent radionuclides, deficiencies of ^{234}Th and ^{210}Po in the euphotic layer were commonly found, indicating evidence for an efficient removal process. A layer with excess ^{234}Th underlying the euphotic layer was found in January 2006, October 2007 and June 2007, which is the result of remineralization (Buesseler et al., 2008). The remineralization phenomenon is also shown as a layer of excess ^{210}Po found in all cruises, except in June and December 2008, corroborating the results from other regions (Bacon et al., 1976; Thomson and Turekian, 1976). As a result of atmospheric deposition, excess ^{210}Pb was commonly observed in the upper 200 m during all cruises, consistent with the findings of Obata et al. (2004) and Chung and Wu (2005).

Assuming steady-state and negligible physical transport, the flux of ^{234}Th out of the euphotic depth can be calculated by Eq. (1).

$$F_{\mathrm{Th}'} = \lambda_{\mathrm{Th}} \int_0^{100} \left({}^{238}\mathrm{U} - {}^{234}\mathrm{Th}_t \right) dz + V, \quad (1)$$

where $F_{\mathrm{Th}}{}'$ is the removal flux, λ_{Th} is radioactive decay constant ($= 0.0287\,\mathrm{d}^{-1}$) and V is the net flux of ^{234}Th from physical transport. To justify the assumption of steady-state, the contribution of temporal changes in ^{234}Th activity concentrations in the mass balance needs to be assessed. It is found that the temporal change is only equivalent to 0.1–3.1 % of the contribution by radioactive decay, which is negligible in the flux calculation. The $F_{\mathrm{Th}}{}'$ caused by physical transport can be evaluated based on the unpublished ^{234}Th data obtained from 6 stations in March and July 2000, which covered 3×3 degree region of the study area. Following the procedures of Liang et al. (2003), the mean current velocity was estimated by averaging the archived shipboard ADCP data collected during 1991–2006. The results showed that horizontal transport by surface currents contributes only 1.5 % of ^{234}Th in the region. Negligible contribution of ^{234}Th from horizontal advection at the SEATS site corroborates to the work conducted by Cai et al. (2008) in the southern South China Sea and by Chen et al. (2008) in the northern shelf of the South China Sea. Based on the distributions of ^{234}Th and ^{228}Th in the upper 500 m, Cai et al. (2006) also concluded that advection/diffusion is not a significant term in the scavenging model.

The flux of ^{210}Pb out of the euphotic depth can be calculated by Eq. (2).

$$F_{\mathrm{Pb}'} = \lambda_{\mathrm{Pb}} \int_0^{100} \left({}^{226}\mathrm{Ra} - {}^{210}\mathrm{Pb}_t \right) dz + I_{\mathrm{Pb}}, \quad (2)$$

where $F_{\mathrm{Pb}}{}'$ is the removal flux, λ_{Pb} is radioactive decay constant of ^{210}Pb ($= 8.48 \times 10^{-5}\,\mathrm{d}^{-1}$) and I_{Pb} is the atmospheric ^{210}Pb deposition flux. The I_{Pb} is about $0.4\,\mathrm{dpm\,cm^{-2}\,a^{-1}}$ according to the model by Feichter et al. (1991). Based on ^{210}Pb chronology in ornithogenic sediments, Xu et al. (2011) estimated the atmospheric ^{210}Pb flux of $0.76\,\mathrm{dpm\,cm^{-2}\,a^{-1}}$ in the southern South China Sea. Here we assume an average I_{Pb} of $0.6\,\mathrm{dpm\,cm^{-2}\,a^{-1}}$ ($16.4\,\mathrm{dpm\,m^{-2}\,d^{-1}}$).

The flux of ^{210}Po out of the euphotic depth is calculated by Eq. (3),

$$F_{\mathrm{Po}'} = \lambda_{\mathrm{Po}} \int_0^{100} \left({}^{210}\mathrm{Pb}_t - {}^{210}\mathrm{Po}_t \right) dz + I_{\mathrm{Po}}, \quad (3)$$

where $F_{\mathrm{Po}}{}'$ is the removal flux, λ_{Pb} is radioactive decay constant of ^{210}Po ($= 0.005\,\mathrm{d}^{-1}$) and I_{Po} is the atmospheric ^{210}Po deposition flux, which is assumed to be 10 % of the atmospheric ^{210}Pb flux (Turekian et al., 1977). Since the spatial variation of ^{210}Po in the surface water of the South China Sea is small (Yang et al., 2006; Wei et al., 2011), as is the case for ^{234}Th, horizontal transport should be negligible. However, similar to the nutrients, the vertical profile of $^{210}\mathrm{Po}_t$ shows evidence for an increase in the thermocline layer, vertical diffusion may play a significant role in the mass balance of ^{210}Po in the euphotic layer (Sarin et al., 1994). Based on the ^{228}Ra profiles, the eddy diffusion coefficient ranges from 0.23 to $1.0\,\mathrm{cm^2\,s^{-1}}$ was estimated in the South China Sea (Cai et al., 2002a, b; Nozaki and Yamamoto, 2001). If an eddy diffusion coefficient of $0.55\,\mathrm{cm^2\,s^{-1}}$ (Nozaki and Yamamoto, 2001) and mean vertical gradient of ^{210}Po between 0 and 300 m were applied to the mass balance equation, the vertical fluxes of ^{210}Po due to upward diffusion would be equivalent to 2–8 % of the total flux, lower than that in oligotrophic North Pacific reported by Verdeny et al. (2008). Hence, the contribution of the vertical diffusion does not need to be included in the flux estimation.

The inventories, deficiencies, and removal fluxes of ^{234}Th, ^{210}Pb, and ^{210}Po in the euphotic layer are summarized in Table 2. Daughter nuclide deficiencies from their parent nuclides resulted in removal fluxes of 1.1×10^3–$1.8 \times 10^3\,\mathrm{dpm\,m^{-2}\,d^{-1}}$ and 7.1–$40.2\,\mathrm{dpm\,m^{-2}\,d^{-1}}$ for ^{234}Th and ^{210}Po, respectively, from the euphotic layer. Due to atmospheric input, an excess of ^{210}Pb relative to ^{226}Ra is commonly observed in the upper water column. As is apparent, the atmospheric input is the dominant source term in Eq. (2), thus, the $F_{\mathrm{Pb}}{}'$ is close to the constant atmospheric ^{210}Pb flux, $16.4\,\mathrm{dpm\,m^{-2}\,d^{-1}}$. No systematic variations were found for the temporal values of $F_{\mathrm{Th}}{}'$, $F_{\mathrm{Pb}}{}'$, and $F_{\mathrm{Po}}{}'$. Based on the ^{210}Pb and ^{210}Po content in the surface water, Nozaki et al. (1998) predicted a ^{210}Po/^{210}Pb ratio of 0.58 in sinking particles from the South China Sea. The ^{210}Po/^{210}Pb ratio 0.4–2.5 in the sinking particles exiting from the euphotic layer that was estimated by this study is within the range of the ^{210}Po/^{210}Pb ratio of 0.4–4.5 measured by our sediment traps.

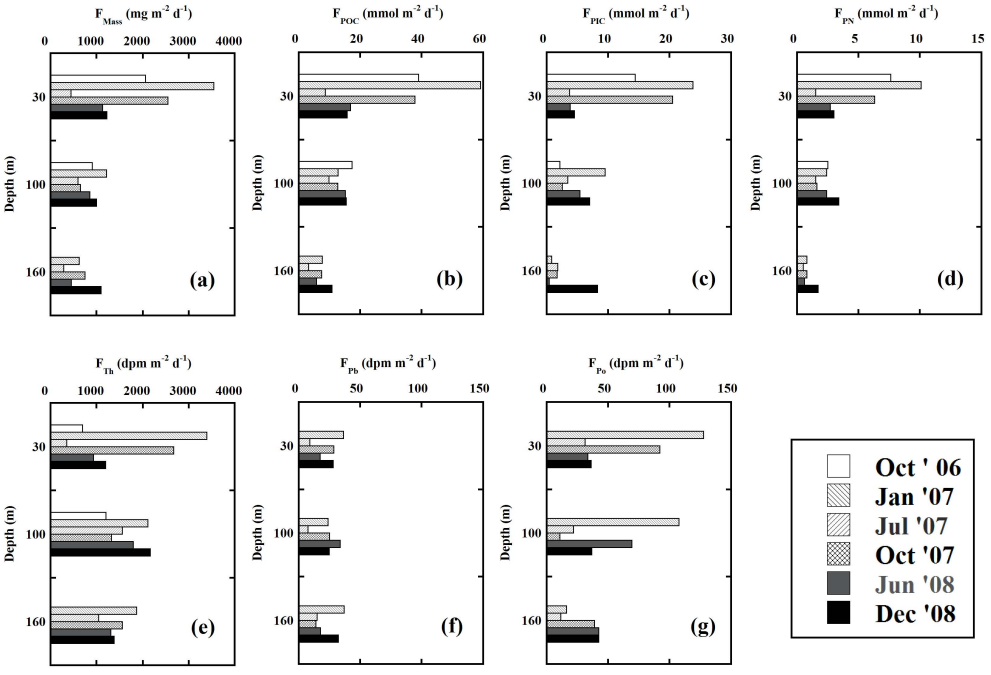

Fig. 5. Fluxes of **(a)** total mass (F_{mass}), **(b)** particulate organic carbon (F_{POC}), **(c)** particulate inorganic carbon (F_{PIC}), **(d)** particulate nitrogen (F_{PN}), **(e)** ^{234}Th (F_{Th}), **(f)** ^{210}Pb (F_{Pb}), and **(g)** ^{210}Po (F_{Po}) measured by the floating traps.

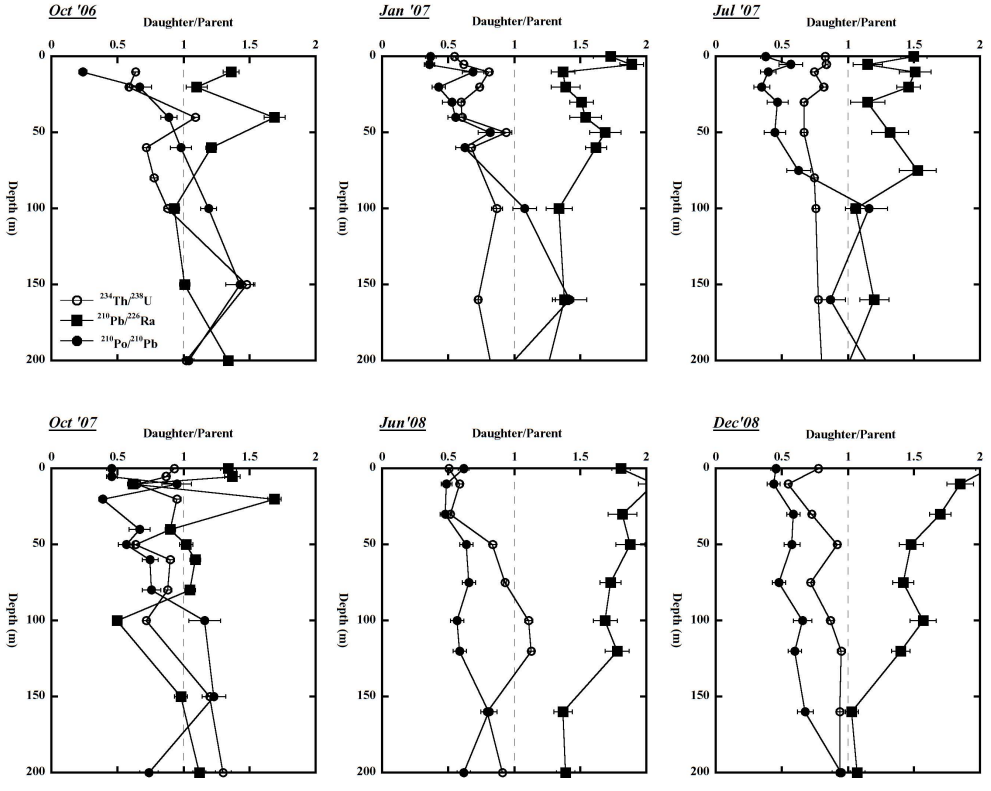

Fig. 6. Vertical distributions of the ratios of total activities of daughter and parent radionuclides obtained from the six cruises. The dotted line represents the secular equilibrium of daughter-parent relationship. Error bars represent uncertainty based on propagated counting errors ($\pm 1\sigma$).

Table 2. Inventories of radionuclides in dissolved and particulate phases of seawater, deficiencies of total activity of daughter with respect to parent radionuclides, and their removal fluxes from the euphotic layer. Uncertainties of various removal fluxes are estimated based on propagated errors ($\pm 1\sigma$).

Cruise	Time	Inventory (dpm m^{-2})						Deficiency (dpm m^{-2})			Removal flux (dpm m^{-2} d^{-1})		
		$^{234}Th_d$	$^{234}Th_p$	$^{210}Pb_d$	$^{210}Pb_p$	$^{210}Po_d$	$^{210}Po_p$	(^{238}U-$^{234}Th_t$)	(^{226}Ra-$^{210}Pb_t$)	($^{210}Pb_t$−$^{210}Po_t$)	F_{Th}'	F_{Pb}'	F_{Po}'
ORI-812*	Oct 2006	191000		7280		6103		50307	−1421	1177	1447 ± 139	16.3 ± 2.4	7.5 ± 2.1
ORI-821	Jan 2007	149 524	37 578	7534	985	3266	2564	55 080	−2925	2690	1584 ± 174	16.2 ± 4.4	15.1 ± 6.8
ORIII-1239	Jul 2007	161 069	14795	7069	415	3529	744	64 557	−1868	3210	1857 ± 174	16.3 ± 5.5	17.7 ± 10.2
ORI-845	Oct 2007	182 687	18 436	5394	741	3465	515	38 424	−278	2156	1105 ± 125	16.4 ± 2.9	12.4 ± 5.0
ORI-866	Jun 2008	152 631	34 811	9555	1003	4792	1325	55 640	−4769	4441	1600 ± 110	16.0 ± 2.7	23.9 ± 6.3
ORI-887	Dec 2008	156 938	24 882	8053	894	3744	1076	56537	−3366	4127	1626 ± 129	16.2 ± 2.8	22.3 ± 7.2

* Inventories of ^{234}Th,^{210}Pb, and ^{210}Po represent total values since the radionuclide activities were measured on unfiltered sample.

4.2 Trapping efficiency determined by ^{234}Th, ^{210}Po, and ^{210}Pb

It is known that the sediment traps can show trapping efficiencies different from 1 (or 100 %), due to hydrodynamic and swimmer effects (Buesseler, 1991; Buesseler et al., 2007), as well as selective dissolution effects (Hung et al., 2010; Xu et al., 2011). To evaluate the trapping efficiency of the floating trap, the ^{234}Th/^{238}U disequilibria in the upper water column are commonly used to assess the trapping efficiency of the floating trap. The ^{234}Th flux measured by the sediment trap deployed at specific depth should be equal to the removal flux calculated from the deficiency in the water column above the depth. Ideally, following the same concept, the comparison of measured with estimated ^{210}Pb and^{210}Po fluxes can also be used as an indicator of trapping efficiency of the floating traps. Hence, we have calculated the trapping efficiencies of the floating traps by the ratios of measured and predicted fluxes of ^{234}Th,^{210}Pb, and ^{210}Po at the three depths. The trapping efficiencies for the six cruises and the average values at the three deployment depths are shown in Table 3. The trapping efficiencies for the traps deployed at 100 m, the euphotic depth, range between 1.06 ± 0.2 and 3.99 ± 3.23 based on ^{234}Th and ^{210}Po data, respectively. Considering the uncertainties associated with sediment trap deployments, these trapping efficiencies are acceptable, as most of the values at 100 and 160 m are close to 1 (Table 3). A large range of trapping efficiency for floating traps, with the ratio of measured and modeled fluxes ranging from 0.1 to 20, is found (Buesseler, 1991; Stewart et al., 2007; Wei and Murray, 1992; Buesseler et al., 2007). A trapping efficiency close to unity and a small variability for the traps deployed at 100 m increase the reliability of the export flux assessment (Buesseler et al., 2007). While it is noted that the traps deployed at 30 m depth, within the surface mixed layer, generally give significantly higher radionuclide fluxes than expected values and reveal a large variability, they also experience greater hydrodynamic effects, which may be the cause for these phenomena. It is also worth noting that, except for the 100 m trap of July 2007, all trapping efficiencies estimated by F_{Po} and F_{Po}' are greater than unity, which may be related to the fast regeneration rate of ^{210}Po due to particle remineralization in the euphotic layer. An elevation of ^{210}Po activity in seawater due to regeneration process was commonly found in the upper water column (Bacon et al., 1976), which results in a lower deficiency of ^{210}Po relative to ^{210}Pb and, hence, a lower F_{Po}'. Compared with the concentrations of trace metal in the same samples (Ho et al., 2010), it was found ^{210}Po content is highly correlated ($r > 0.8$, $n = 11$) with biophilic elements, P, S, Ca, Zn, Mo, and Cd. Previous studies have shown that ^{210}Po, a sulfur analog found mostly associated with proteins (Fisher et al., 1983), shows higher affinity toward organic particles than ^{210}Pb (Bacon et al., 1976; Shannon et al., 1970), and thus, ^{210}Po is more sensitive to particle decomposition processes than ^{234}Th (Stewart et al., 2007), which is mostly surface-bound (Santschi et al., 2006).

4.3 Export fluxes of POC, PIC, and PN estimated by radionuclide tracers

Export fluxes of POC, PIC, and PN can be indirectly estimated if the ratio of the concentration of carbon and nitrogen to the radionuclides in sinking particles are known. Since the first study in the Panama Basin (Murray et al., 1989), ^{234}Th has been extensively used in the past two decades as a powerful tracer for estimating the export production (i.e. POC flux) from the euphotic layer of the ocean (Buesseler et al., 2006 and refereces therein). For the same purpose, ^{210}Pb and ^{210}Po, as additional tracers, were used to constrain the determination of the export production in the euphotic layer (Shimmield et al., 1995; Stewart et al., 2007; Murray et al., 2005; Friedrich and Rutgers van der Loeff, 2002; Kim and Church, 2001; Buesseler et al., 2008). In the context of treating particle-reactive radionuclides as proxies for POC flux, export production or sinking flux of PIC and PN from the euphotic layer can also be estimated by multiplying the flux of radionuclides, which is obtained from the mass balance of daughter radionuclide relative to its parent radionuclide in the euphotic layer, by the ratio of POC (or PIC, PN) and radionuclide in sinking (or sinkable) particles (Murray et al.,

Table 3. Trapping efficiencies estimated by the ratios of measured and modeled fluxes of ^{234}Th, ^{210}Pb, and ^{210}Po from the three depths for all cruises. Average value, standard deviation, and relative standard deviation for each depth are listed.

	Depth (m)	Oct. 2006	Jan. 2007	Jul. 2007	Oct. 2007	Jun. 2008	Dec. 2008	Av. s.d.	r.s.d.
F_{Th}: F_{Th}'	30	1.12	5.29	0.79	8.39	0.98	0.75	2.89 ± 3.22	112 %
	100	0.83	1.33	0.84	1.19	1.12	1.06	1.06 ± 0.20	19 %
	160		0.91	0.37	1.26	0.81	1.18	0.91 ± 0.35	39%
F_{Pb}: F_{Pb}'	30		1.33	0.83	2.60	1.61	1.02	1.48 ± 0.69	47 %
	100		0.87	0.69	2.29	3.21	0.89	1.59 ± 1.11	70 %
	160		1.37	1.38	1.27	1.69	1.15	1.37 ± 0.20	15%
F_{Po}: F_{Po}'	30		15.02	2.77	17.85	4.11	5.26	9.00 ± 6.91	77 %
	100		7.64	0.75	1.15	3.35	7.07	3.99 ± 3.23	81 %
	160		2.77	0.39	4.22	1.36	7.84	3.32 ± 2.92	88 %

2005; Buesseler, 1998; Bacon et al., 1996), i.e.

$$F'_{POC-RN} = F'_{RN} \times (\frac{POC}{RN}), \quad (4)$$

$$F'_{PIC-RN} = F'_{RN} \times (\frac{PIC}{RN}), \quad (5)$$

$$F'_{PN-RN} = F'_{RN} \times (\frac{PN}{RN}), \quad (6)$$

where RN is the abbreviation of radionuclide (^{234}Th, ^{210}Pb, ^{210}Po), F_{POC-RN}', F_{PIC-RN}', and F_{PN-RN}' are fluxes of POC, PIC, and PN estimated by RN as proxy, respectively, F_{RN}' is the flux of radionuclide calculated from the deficiencies of RN in the euphotic layer by Eqs. (1) and (3), and POC/RN , PIC/RN, and PN/RN is the ratio of POC, PIC, and PN and the radionuclides in sinking (or sinkable) particles collected at the euphotic depth. Equations (4) and (6) were previously used for ^{234}Th data to estimate the export flux of POC and PN from the euphotic layer of the Atlantic Ocean (Buesseler et al., 1992; Amiel et al., 2002) and the Pacific Ocean (Murray et al., 1996). Limited by the scarcity of sediment trap data on radionuclide to PIC ratios, very few applications of Eq. (5) on PIC export exist. The only application of using ^{234}Th as a PIC proxy is Bacon et al. (1996), who estimated PIC export fluxes based on PIC/^{234}Th ratios in filtered particles in the Equatorial Pacific.

The POC/RN, PIC/RN, and PN/RN in sinking particles collected at the three depths are shown in Fig. 7. The POC/^{234}Th ratios in sinking particles decreased with depth, with average values of 23.9 ± 16.3, 8.7 ± 3.2, and 4.8 ± 1.8 µmol dpm^{-1} at 30, 100, and 160 m, respectively. The decreasing trend with depth can be attributed to preferential remineralization of organic carbon when particles settle through the water column (Rutgers van der Loeff et al., 2002; Buesseler et al., 2006). Decreasing of POC/^{234}Th ratio with depth were also found for suspended particles in the northern South China Sea by Cai et al. (2008) and Chen et al. (2008). A larger variability of this ratio was found at the mixed layer depth, which may be caused by a more active biological activity in the surface layer. It is noted here that the POC/^{234}Th ratio in sinking particles collected at the euphotic depth falls in a small range and values are similar to those reported for more productive regions, e.g. Northern Atlantic (Buesseler et al., 1992) and higher than in the oligotrophic open ocean, e.g. HOTS and BATS (see the compilation of Buesseler et al., 2006). Due to the low scatter of POC/^{234}Th ratio at the euphotic depth, the export production based on Eq. (4) tends to be less variable (Buesseler et al., 2006). Except during July 2007, the POC/^{210}Pb ratio in sinking particles also shows a decreasing trend with depth (Fig. 7b). The average POC/^{210}Pb ratios are 1088 ± 403, 686 ± 352, and 321 ± 131 µmol dpm^{-1} at 30, 100, and 160 m, respectively. These values are comparable to POC/^{210}Pb ratios of 80–268 µmol dpm^{-1} in sinking particles collected by sediment traps at 150 m off the east coast of the United States (Biscaye et al., 1988) and 50–489 µmol dpm^{-1} in the northwestern Mediterranean (Tateda et al., 2003). The POC/^{210}Po ratios in the sinking particles are highly variable, ranging from 120 to 1200 µmol dpm^{-1}, similar to ratios in the sinking particles collected in the coastal Mediterranean Sea (Tateda et al., 2003; Stewart et al., 2007). However, compared to open ocean values (Verdeny et al., 2008 and references therein), our data fall on the high end of these POC/^{210}Po ratios. Different from ^{234}Th and ^{210}Pb, no systematic trends with depth were found for POC/^{210}Po ratios.

Values of the PIC/^{234}Th (Fig. 7d) and PN/^{234}Th (Fig. 7g) ratios show temporal and vertical variations similar to those of POC/^{234}Th, suggesting no preferential association of ^{234}Th with different components of biological particles. The average PIC/^{234}Th ratios are 8.9 ± 6.3, 2.8 ± 1.1, and 1.9 ± 2.4 µmol dpm^{-1} at 30, 100, and 160 m depth, respectively. These ratios are comparable to the limited published sediment trap data, e.g. 0.6 µmol dpm^{-1} at 300 m in the Northwest Mediterranean (Szlosek et al., 2009). The

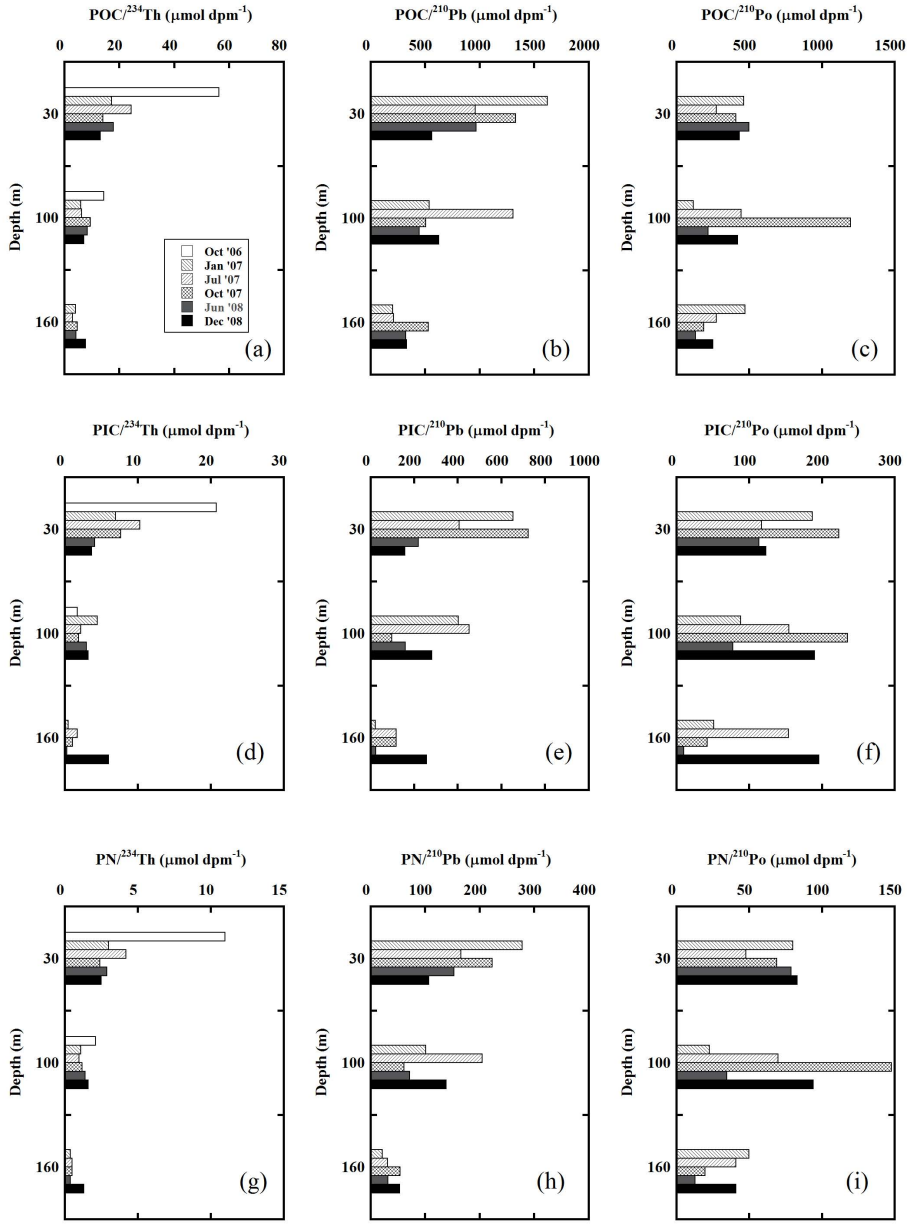

Fig. 7. Ratios of **(a–c)** POC and RN, **(d–f)** PIC and RN, and **(g–i)** PN and RN in settling particles collected by floating traps at the three depths of SEATS.

PN/^{234}Th ratios in the lower euphotic zone range between 0.6 and 1.4 μmol dpm^{-1}, which is similar to 0.7–1.3 μmol dpm^{-1} in the Northern Atlantic (Buesseler et al., 1992). Like ^{234}Th data, the PIC/^{210}Pb (Fig. 7e) and PN/^{210}Pb (Fig. 7h) ratios also show temporal and vertical variations similar to those of POC/^{210}Pb. The PIC/^{210}Pb ratios are 433 ± 252, 279 ± 51, and 108 ± 96 μmol dpm^{-1} at 30, 100, and 160 m, respectively. The ratios at the lower euphotic depth were very similar to 135–518 μmol dpm^{-1} at 150 m in the Northwest Mediterranean (Tateda et al., 2003). The PN/^{210}Pb ratios obtained from this study are comparable with the ratios in sinking particles from the euphotic layer in the Mid Atlantic Bight (21∼279 mmol dpm-1, Biscaye et al., 1988) and the Northwest Mediterranean (4–126 mmol dpm-1, Tateda et al., 2003). Both PIC/^{210}Po (Fig. 7f) and PN/^{210}Po (Fig. 7i) ratios show large seasonal and vertical variability. The average PIC/^{210}Po and PN/^{210}Po ratios range from 91 to 433 μmol dpm^{-1} and 14 to 50 μmol dpm^{-1}, respectively. Compared to the trap data and PIC, PN, and ^{210}Po data of Tateda et al. (2003), our results fall in the

same range as the PIC/^{210}Po and PN/^{210}Po ratios from the coastal Mediterranean, i.e. 94–1115 µmol dpm^{-1}and 7–148 µmol dpm^{-1}, respectively.

Using the ratios of POC, PIC, and PN to the three radionuclides in sinking particles of the 100 m trap, the export fluxes of organic carbon, inorganic carbon, and nitrogen via particle settling from the euphotic layer can be calculated by Eqs. (4)-(6) and plotted for different cruises in Fig. 8. Along with the estimated fluxes based on the three radionuclide proxies, directly measured fluxes of POC, PIC, and PN by sediment traps deployed at 100 m are also shown in the figure. The export fluxes of POC, PIC, and PN from the euphotic layer of the northern South China Sea determined by various approaches are discussed in the following section.

4.4 Comparison of export fluxes by different approaches

As can be seen from Fig. 8, values of $F_{\mathrm{POC-Th}}{}'$ display a remarkable resemblance to F_{POC} values, both in terms of magnitude and temporal variation. The $F_{\mathrm{POC-Th}}{}'$ ranges from 9.6 mmol-C m^{-2} d^{-1} to 21.0 mmol-C m^{-2} d^{-1} and the F_{POC} ranges from 9.8 to 18.5 mmol-C m^{-2} d^{-1}. The temporal variation of both F_{POC} and $F_{\mathrm{POC-Th}}{}'$ generally corroborates with the seasonal variation of primary productivity at SEATS (Tseng et al., 2005). In the region further south to SEATS, Cai et al. (2008), using a 3-D scavenging model, estimated the POC export ranged from −10.7 to 12.6 mmol-C m^{-2} d^{-1} calculated from ^{234}Th deficiencies and POC/^{234}Th ratios in pump-collected particles. They attributed the negative values at some stations in the study area to large input of particulate matter by horizontal transport. Although ^{210}Pb has been found useful in estimating the POC sinking flux in the deep ocean (Moore and Dymond, 1988), there are very few studies using the ^{210}Pb/^{226}Ra disequilibrium to estimate the export production in the euphotic layer because a reliable atmospheric ^{210}Pb flux is not available to better constrain the source term in Eq. (2), which is much greater than the input from the radioactive decay of ^{226}Ra. Nonetheless, assuming the atmospheric ^{210}Pb flux of 0.6 dpm cm^{-2} a^{-1} (Feichter et al., 1991; Xu et al., 2010), the $F_{\mathrm{POC-Pb}}{}'$ of 7.2–21.3 mmol-C m^{-2} d^{-1} can be estimated, which is within the range of F_{POC} and $F_{\mathrm{POC-Th}}{}'$ values. Since a constant atmospheric ^{210}Pb flux is assumed, the $F_{\mathrm{Pb}}{}'$ values show no seasonal variation (Table 2). Hence, the temporal variations of the $F_{\mathrm{POC-Pb}}{}'$ are resulting from the POC/^{210}Pb ratio in sinking particles, which may be affected by particle composition. The $F_{\mathrm{POC-Po}}{}'$ based on the ^{210}Po-^{210}Pb system showed the largest range of POC export, ranging from 1.8 to 20.3 mmol-C m^{-2} d^{-1}, among the three pairs of disequilibria.

Verdeny et al. (2009) recently presented a review of previous studies using ^{234}Th and ^{210}Po as dual tracers to estimate the export production in the ocean. A discrepancy between the POC fluxes estimated by ^{234}Th-^{238}U and ^{210}Po-^{210}Pb disequilibria was commonly found. For example, the export production deduced from the ^{210}Po deficiency was two folds higher than that estimated from the ^{234}Th-^{238}U disequilibrium in the Atlantic (Sarin et al., 1994). On the other hand, Shimmield et al. (1995) found the export production estimated by the $F_{\mathrm{POC-Po}}{}'$ was an order of magnitude lower than that estimated from the $F_{\mathrm{POC-Th}}{}'$ values in the marginal ice zone of the Antarctica. In the Equatorial Pacific, Murray et al. (2005) reported a generally higher and more variable $F_{\mathrm{POC-Po}}{}'$ than $F_{\mathrm{POC-Th}}{}'$ values. Stewart et al. (2007) obtained the $F_{\mathrm{POC-Th}}{}'$ and $F_{\mathrm{POC-Po}}{}'$ values of 3.8–8.9 mmol-C m^{-2} d^{-1} and 1.2–2.6 mmol-C m^{-2} d^{-1}, respectively, from the euphotic layer of the Northwestern Mediterranean. Recently, Buesseler et al. (2008) used ^{234}Th and ^{210}Po proxies to estimate POC export fluxes from the euphotic layer of the Sargasso Sea and found the $F_{\mathrm{POC-Po}}{}'$ is about two folds higher than the $F_{\mathrm{POC-Th}}{}'$. Hence, considering the intrinsic difference in half-life, source function, and geochemical characteristics among the three radionuclides and the uncertainty associated with the scavenging model, the POC

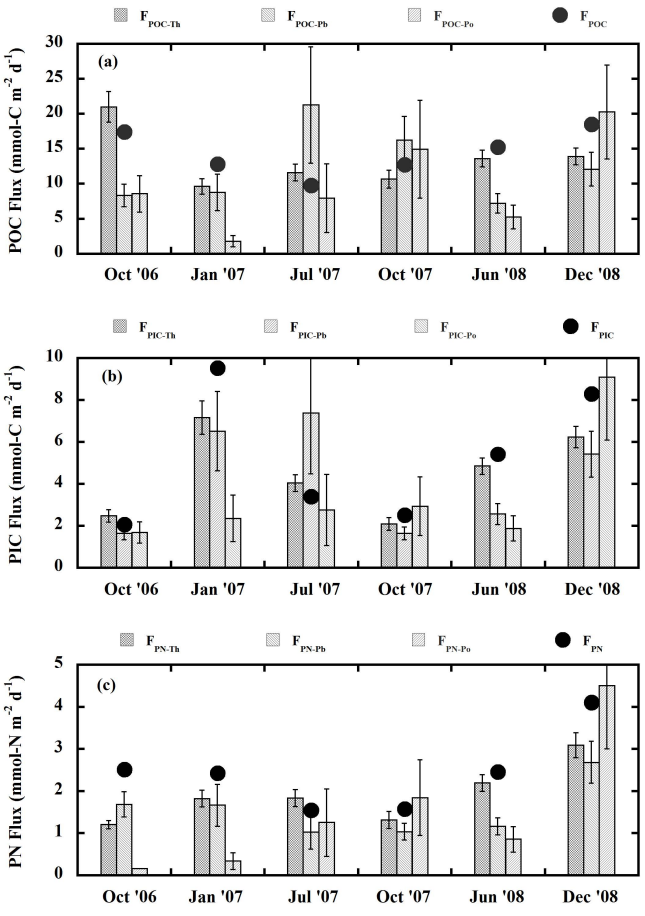

Fig. 8. Export fluxes of **(a)** POC, **(b)** PIC, and **(c)** PN estimated by ^{234}Th, ^{210}Pb, and ^{210}Po as proxy (bars) and measured by the floating traps (circles) from the euphotic layer. Error bars represent uncertainty based on propagated counting errors ($\pm 1\sigma$).

Table 4. Export production estimated by various methods in the South China Sea. Average and standard deviation of various fluxes from this study are shown in parentheses.

Method	mmol-C m^{-2} d^{-1}	Reference	Note
Northern shelf			
^{234}Th proxy	5.3∼26.6	Chen et al. (2008)	Estimated POC flux at 100 m
Central basin			
^{228}Ra-NO_3 coupling	26.5	Nozaki and Yamamoto (2001)	Estimated diffusive NO_3 flux at 100 m
Biogeochemical modeling	1.7∼3.5	Liu et al. (2002)	Estimated POC flux at 125 m
^{15}N new production	3.8 ∼ 6.7	Chen (2005)	
Carbon budget	2.9 ∼ 6.7	Chou et al. (2006)	Net community production at mixed depth
Moored sediment trap	4.2 ∼ 71.8	Ho et al. (2009)	Estimated by phosphorus flux at 160 m
Moored sediment trap	3.3 ∼ 55.0	Ho et al. (2011)	Measurement of POC flux at 120 m
Floating trap	9.8 ∼ 18.5 (14.4 ± 3.3)	This study	Measurement of POC flux at 100 m
^{234}Th proxy	9.6 ∼ 21.0 (13.4 ± 4.1)		Estimated POC flux at 100 m
^{210}Pb proxy	7.2 ∼ 21.3 (12.3 ± 5.5)		Estimated POC flux at 100 m
^{210}Po proxy	1.8 ∼ 20.3 (9.8 ± 6.7)		Estimated POC flux at 100 m
Southern shelf			
^{228}Ra-NO_3 coupling	4.4 ∼ 5.7	Cai et al. (2002a, b)	Estimated diffusive NO_3 flux at 200 m
^{234}Th proxy	5.7		Estimated POC flux at 100 m
^{228}Th proxy	1.7		Estimated POC flux at 100 m
^{210}Po proxy	1.2	Yang et al. (2009)	

fluxes estimated by these proxies in our work a consistent estimate of the export production in the Northern South China Sea.

There is some literature that estimated the export production by various other approaches in the Northern South China Sea. These approaches include a $^{228}Ra/NO_3$ coupled model (Nozaki and Yamamoto, 2001), biogeochemical modeling (Liu et al., 2002), carbon budgeting (Chou et al., 2006), ^{15}N incubation measurements of new production (Chen and Chen, 2005; 2004), and phosphorus flux measurements by sediment traps (Ho et al., 2009). The export fluxes by these approaches are summarized in Table 4. The export productions estimated by various proxies in the other regions of the South China Sea, including the northern shelf (Chen et al., 2008) and the southern shelf (Cai et al., 2002a, b; Yang et al., 2009), are also listed in the table. Among these studies, based on the *P* fluxes measured by the sediment traps deployed at the depth underlying the euphotic layer, Ho et al. (2009) obtained the largest range of export fluxes (4.2–70.8 mmol-C m^{-2} d^{-1}) at the SEATS. Some anomalously high fluxes reported by Ho et al. (2009) may be caused by over-trapping of their sediment traps, which were deployed at 160 m on a long mooring line. An even larger range of POC flux, ranging from 3.3 to 55 mmol-C m^{-2} d^{-1}, was measured at 120 m by moored sediment traps (Ho et al., 2011). It can thus be concluded that the export production can be reasonably estimated by using ^{234}Th, ^{210}Pb, and ^{210}Po as carbon proxies in sinking particles.

The correlation of POC exports obtained by various methods and integrated primary production during the six cruises is shown in Fig. 9. The primary production varied from 9.5 mmol-C m^{-2} d^{-1} in July 2007 to 46.1 mmol-C m^{-2} d^{-1} in October 2007. The export efficiency can be indicated by the ratio of the POC exports and the primary production (Buesseler, 1998), which showed a large range between 0.04 and 2.17 with an average ratio of 0.53. The unreasonably high ratios greater than unity were found for ORIII-1239, from which the primary production was suspected to be underestimated based on the vertical profile of primary productivity. It is found that most of data fall in the range of 0.2 and 0.7, which implies that export efficiency is high in the South China Sea.

The values of F_{PIC} range from 2.1 to 9.5 mmol-C m^{-2} d^{-1} (Fig. 8b), which is significantly higher than in other regions (Berelson et al., 2007). The temporal variation of the F_{PIC} is generally predicted by the fluxes estimated from the other proxies. Based on the ^{234}Th deficiency and the PIC/^{234}Th ratio in pump-collected large particles, Bacon et al. (1996) estimated a PIC export of 0.45–0.80 mmol-C m^{-2} d^{-1} at 150 m and 0.54–0.71 mmol-C m^{-2} d^{-1} at 200 m in the Equatorial Pacific. High F_{PIC} values at SEATS may be attributed to the dominant coccolithophores in the algal community during the winter season in the South China Sea (Chen and Chen, 2005), which enhances the sinking flux due to a ballast effect. Indeed, microscopic examination of trap particles shows that skeletal remains of coccolithophorids and diatoms are abun-

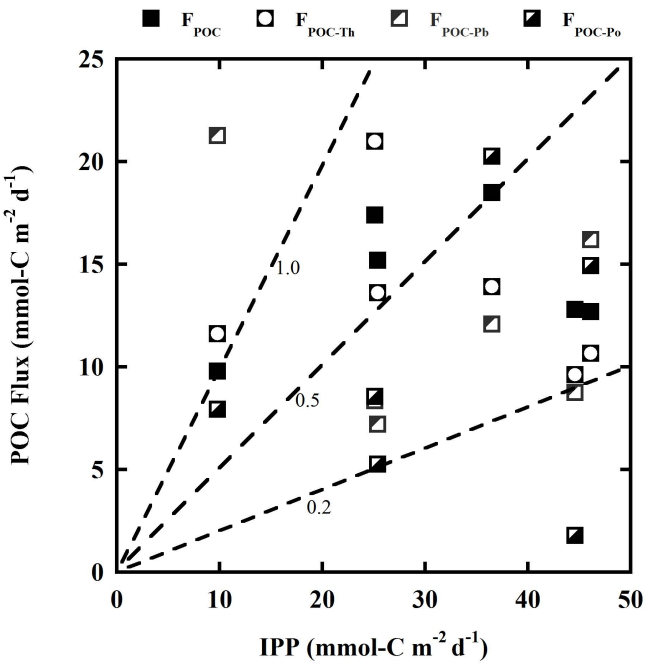

Fig. 9. Correlation of F_{POC}, F_{POC-Th}', F_{POC-Pb}', and F_{POC-Po}' with integrated primary productivity (IPP). Export ratios of 0.2 and 0.5 are shown by dashed lines.

dant during the winter cruises (ORI-821 and ORI-887) (Ho et al., 2010). Calculated from the temporal change of the inventory of alkalinity in the euphotic layer during October 2006 and December 2008, a PIC production ranging from 0.4 to 11.4 mmol-C m^{-2} d^{-1} can be estimated. Direct measurements of Ca concentration from the same samples shows F_{PIC} ranging from 1.6 to 6.2 mmol-C m^{-2} d^{-1} (Ho et al., 2010). All the F_{PIC}, F_{PIC-Th}', F_{PIC-Pb}', and F_{PIC-Po}' values are thus within the PIC production estimates, indicating the PIC export flux was reliably estimated.

The F_{PN} values measured at 100 m of the SEATS ranged from 1.5 mmol-N m^{-2} d^{-1} in July 2007 to 4.1 mmol-N m^{-2} d^{-1} in December 2008, very close to the flux of ~2 mmol-N m^{-2} d^{-1} derived from a $^{228}Ra/NO_3$ coupled model at the site about 300 km to the south of our station (Nozaki and Yamamoto, 2001). Except for the F_{PN-Po}' in October 2006 and January 2007, the values of F_{PN-Th}', F_{PN-Pb}', and F_{PN-Po}' are close to the F_{PN} within a factor of three. The export of nitrogen via particle settling in the Northern South China Sea is also close to the measured PN flux of 1.2–2 mmol-N m^{-2} d^{-1} in the North Atlantic (Martin et al., 1993) and the northeast Pacific (Wong et al., 1999).

5 Conclusions

Temporal data of dissolved and particulate concentrations and fluxes of the particle-reactive radionuclides, ^{234}Th, ^{210}Pb, and ^{210}Po, in the upper water column of the time-series station, SEATS (18° N, 116° E) were obtained during 2006 to 2008. All fluxes (total mass, ^{234}Th, ^{210}Pb, ^{210}Po, POC and PIC) measured at the euphotic depth were lower in summer-fall and higher in winter-spring, reflecting the seasonal variability of biological pumping. Using the three radionuclides as proxies, the disequilibria of $^{234}Th/^{238}U$, $^{210}Pb/^{226}Ra$, and $^{210}Po/^{210}Pb$ were combined with their ratios to POC, PIC, and PN in the sinking particles collected at the euphotic depth to estimate export production in the Northern South China Sea. Our results showed that estimated fluxes by the radionuclide proxies are within the range of those measured by sediment traps, which ranged from 1.8 to 21.3 mmol-C m^{-2} d^{-1}, from 1.6 to 9.1 mmol-C m^{-2} d^{-1}, and from 0.2 to 4.5 mmol-N m^{-2} d^{-1}, for POC, PIC, and PN, respectively.

Acknowledgements. This study was supported by the National Science Council under grants NSC 99-2611-M-002 -004. We are grateful to W.-H. Lee and F.-S. Kuo for help in sampling. We would also like to thank the technical group of the SEATS program of NCOR for their excellent work in measuring the hydrographic parameters. The manuscript benefited from the constructive reviews by P. Cai and an anonymous reviewer.

Edited by: F. Chai

References

Amiel, D. J., Cochran, K., and Hirschberg, D. J.: $^{234}Th/^{238}U$ disequilibrium as an indicator of the seasonal export flux of particulate organic carbon in the North Water, Deep-Sea Res. II, 49, 5191–5209, 2002.

Bacon, M. P., Spencer, D. W., and Brewer, P. G.: $^{210}Pb/^{226}Ra$ and $^{210}Po/^{210}Pb$ disequilibria in seawater and suspended particulate matter, Earth Planet. Sci. Lett., 32, 277–299, 1976.

Bacon, M. P., Cochran, J. K., Hirschberg, D., Hammar, T. R., and Fleer, A. P.: Export flux of carbon at the equator during the EqPac time-series cruises estimated from ^{234}Th measurements, Deep-Sea Res. II, 43, 1133–1153, 1996.

Berelson, W. M., Balch, W. M., Najjar, R., Feely, R. A., Sabine, C., and Lee, K.: Relating estimates of CaCO3 production, export, and dissolution in the water column to measurements of CaCO3 rain into sediment traps and dissolution on the sea floor: A revised global carbonate budget, Global Biogeochem. Cy., 21, GB1024, doi:10.1029/2006GB002803, 2007.

Buesseler, K. O.: Do upper-ocean sediment traps provide an accurate record of particle flux?, Nature, 353, 420–423, 1991.

Buesseler, K. O.: The decoupling of production and particulate export in the surface ocean, Global Biogeochem. Cy., 12, 297–310, 1998.

Biscaye, P. E., Anderson, R. F., and Deck, B. L.: Fluxes of particles and constituents to the eastern United States continental slope and rise: SEEP-I, Cont. Shelf Res., 8, 855–904, 1988.

Buesseler, K. O., Bacon, M. P., Cochran, J. K., and Livingston, H. D.: Carbon and nitrogen export during the JGOFS North Atlantic Bloom Experiment estimated from ^{234}Th: ^{238}U disequilibrium, Deep-Sea Res. I, 39, 1115–1137, 1992.

Buesseler, K. O., Benitez-Nelson, C. R., Moran, S. B., Burd, A., Charette, M., Cochran, J. K., Coppola, L., Fisher, N. S., Fowler, S. W., Gardner, W. D., Guo, L. D., Gustafsson, O., Lamborg, C., Masqué, P., Miquel, J. C., Passow, U., Santschi, P. H., Savoye, N., Stewart, G., and Trull, T.: An assessment of particulate organic carbon to thorium-234 ratios in the ocean and their impact on the application of ^{234}Th as a POC flux proxy, Mar. Chem., 100, 213–233, 2006.

Buesseler, K. O., Antia, A. N., Chen, M., Fowler, S. W., Gardner, W. D., Gustafsson, O., Harada, K., Michaels, A. F., Rutgers van der Loeff, M., Sarin, M., Steinberg, D. K., and Trull, T.: An assessment of the use of sediment traps for estimating upper ocean particle fluxes, J. Mar. Res., 65, 345–416, 2007.

Buesseler, K. O., Lamborg, C., Cai, P., Escoube, R., Johnson, R., Pike, S., Masqué, P., McGillicuddy, D., and Verdeny, E.: Particle fluxes associated with mesoscale eddies in the Sargasso Sea, Deep-Sea Res. II, 55, 1426–1444, doi:10.1016/j.dsr2.2008.02.007, 2008.

Cai, P., Huang, Y., Chen, M., Liu, G., and Qiu, Y.: New production in the South China Sea, Science in China (series D), 45, 103–109, 2002a.

Cai, P., Huang, Y. P., Chen, M., Guo, L. D., Liu, G. S., and Qiu, Y. S.: New production based on ^{228}Ra-derived nutrient budgets and thorium-estimated POC export at the intercalibration station in the South China Sea, Deep-Sea Res. I, 49, 53–66, 2002b.

Cai, P., Chen, W., Dai, M., Wan, Z., Wang, D., Li, Q., Tang, T., and Lv, D.: A high-resolution study of particle export in the Southern South China Sea based on ^{234}Th:^{238}U disequilibrium, J. Geophys. Res., 113, C04019, doi:10.1029/2007JC004268, 2008.

Cai, P. H., Dai, M. H., Chen, W. F., Tang, T. T., and Zhou, K. B.: On the importance of the decay of Th-234 in determining size-fractionated C/Th-234 ratio on marine particles, Geophys. Res. Lett., 33, L23602, doi:10.1029/2006gl027792, 2006.

Chen, W., Cai, P., Dai, M., and Wei, J.: ^{234}Th/^{238}U disequilibrium and particulate organic carbon export in the Northern South China Sea, J. Oceanogr., 64, 417–428, 2008.

Chen, Y. L. L., Chen, H. Y., Karl, D. M., and Takahashi, M.: Nitrogen modulates phytoplankton growth in spring in the South China Sea, Cont. Shelf Res., 24, 527–541, doi:10.1016/j.csr.2003.12.006, 2004.

Chen, Y. L. L. and Chen, H. Y.: Spatial and seasonal variations of nitrate based new production and primary production in the South China Sea, Deep-Sea Res. I, 52, 319–340, 2005.

Cherry, R. D., Fowler, S. W., Beasley, T. M., and Heyraud, M.: Polonium-210: Its vertical oceanic transport by zooplankton metabolic activity, Mar. Chem., 3, 105–110, 1975.

Chou, W.-C., Chen, Y.-L. L., Sheu, D. D., Shih, Y.-Y., Han, C.-A., Cho, C. L., Tseng, C.-M., and Yang, Y.-J.: Estimated net community production during the summertime at the SEATS time-series study site, Northern South China Sea: Implications for nitrogen fixation, Geophys. Res. Lett., 33, L22610, doi:10.1029/2005GL025365, 2006.

Chung, Y. and Wu, T.: Large ^{210}Po deficiency in the Northern South China Sea, Cont. Shelf Res., 25, 1209–1224, 2005.

Feichter, J., Brost, R. A., and Heimann, M.: 3-dimensional modeling of the concentration and deposition of Pb-210 aerosols, J. Geophys. Res., 96, 22447–22460, 1991.

Fisher, N. S., Burns, K. A., Cherry, R. D., and Heyraud, M.: Accumulation and cellular distribution of ^{241}Am, ^{210}Po, and ^{210}Pb in two marine algae, Mar. Ecol. Prog. Ser., 11, 233–237, 1983.

Friedrich, J. and Rutgers van der Loeff, M. M.: A two-tracer (^{210}Po-^{234}Th) approach to distinguish organic carbon and biogenic silica export flux in the Antarctic Circumpolar Current, Deep-Sea Res. I, 49, 101–120, 2002.

Ho, T.-Y., You, C.-F., Chou, W.-C., Pai, S.-C., Wen, L.-S., and Sheu, D. D.: Cadmium and phosphorus cycling in the water column of the South China Sea: The roles of biotic and abiotic particles, Mar. Chem., 115, 125–133, 2009.

Ho, T.-Y., Chou, W.-C., Wei, C.-L., Lin, H.-L., and Wong, G. T. F.: Trace metal cycling in the surface water of the South China Sea: Vertical fluxes and sources, Limnol. Oceanogr., 55, 1807–1820, 2010.

Ho, T.-Y., Chou, W.-C., Lin, H.-L., and Sheu, D. D.: Trace metal cycling in the deep water of the South China Sea: The composition, sources, and fluxes of sinking particles, Limnol. Oceanogr., 56, 1225–1243, 2011.

Hung, C.-C., Xu, C., Santschi, P. H., Zhang, S., Schwehr, K. A., Quigg, A., Pinckney, J., Long, R., Guo, L., Gong, G.-C., and Wei, C.-L.: Comparative evaluation of sediment-trap and ^{234}Th-derived POC fluxes from the upper oligotrophic ocean in the Gulf of Mexico and the East China Sea, Mar. Chem., 121, 132–144, 2010.

Kim, G. and Church, T. M.: Seasonal biogeochemical fluxes of ^{234}Th and ^{210}Po in the upper Sargasso Sea: Influence from atmospheric iron deposition, Global Biogeochem. Cy., 15, 651–661, 2001.

Ku, T. L., Knauss, K. G., and Mathiew, G. G.: Uranium in open ocean: concentration and isotopic composition, Deep-Sea Res., 24, 1005–1017, 1977.

Liang, W.-D., Tang, T.-Y., Yang, Y.-J., Ko, M.-T., and Chuang, W.-S.: Upper-ocean currents around Taiwan, Deep-Sea Res. II, 50, 1085–1105, 2003.

Liu, K.-K., Chao, S.-Y., Shaw, P.-T., Gong, G.-C., Chen, C.-C., and Tang, T.-Y.: Monsoon-forced chlorophyll distribution and primary production in the South China Sea: Observations and a numerical study, Deep-Sea Res., 49, 1387–1412, 2002.

Martin, J. H., Fitzwater, S. E., Gordon, R. M., Hunter, C. N., and Tanner, S. J.: Iron, primary production and carbon-nitrogen flux studies during the JGOFS North Atlantic Bloom Experiment, Deep-Sea Res. II, 40, 115–134, 1993.

Moore, W. S. and Dymond, J.: Correlation of Pb-210 removal with organic carbon fluxes in the Pacific Ocean, Nature, 331, 339–341, 1988.

Murray, J. W., Downs, J. N., Strom, S., Wei, C.-L., and Jannasch, H. W.: Nutrient assimilation, export production and ^{234}Th scavenging in the Eastern Equatorial Pacific, Deep-Sea Res., 36, 1471–1489, 1989.

Murray, J. W., Young, J., Newton, J., Dunne, J., Chapin, T., Paul, B., and McCarthy, J. J.: Export flux of particulate organic carbon from the central equatorial Pacific determined using a combined drifting trap-^{234}Th approach., Deep-Sea Res. II, 43, 1095–1132, 1996.

Murray, J. W., Paul, B., Dunne, J. P., and Chapin, T.: ^{234}Th, ^{210}Pb, ^{210}Po and stable Pb in the central equatiorial Pacific: Tracers for

particle cycling, Deep-Sea Res. I, 52, 2109–2139, 2005.

Nozaki, Y. and Yamamoto, Y.: Radium 228 based nitrate fluxes in the eastern Indian Ocean and the South China Sea and a silicon-induced "alkalinity pump" hypothesis, Global Biogeochem. Cy., 15, 555–567, 2001.

Nozaki, Y., Dobashi, F., Kato, Y., and Yamamoto, Y.: Distribution of Ra isotopes and the ^{210}Pb and ^{210}Po balance in surface seawaters of the mid Northern Hemisphere, Deep-Sea Res. I, 45, 1263–1284, 1998.

Obata, H., Nozaki, Y., Alibo, D. S., and Yamamoto, Y.: Dissolved Al, In and Ce in the eastern Indian Ocean and the Southeast Asian Seas in comparison with the radionuclides ^{210}Pb and ^{210}Po, Geochim. Cosmochim. Acta, 68, 1035–1048, 2004.

Rutgers van der Loeff, M. M., Buesseler, K. O., Bathmann, U., Hense, I., and Andrews, J.: Comparison of carbon and opal export rates between summer and spring bloom periods in the region of the Antarctic Polar Front, SE Atlantic, Deep-Sea Res. II, 49, 3849–3870, 2002.

Santschi, P. H., Murray, J. W., Baskaran, M., Benitez-Nelson, C. R., Guo, L. D., Hung, C. C., Lamborg, C., Moran, S. B., Passow, U., and Roy-Barman, M.: Thorium speciation in seawater, Mar. Chem., 100, 250–268, doi:10.1016/j.marchem.2005.10.024, 2006.

Sarin, M. M., Krishnaswami, S., Ramesh, R., and Somayalulu, B. L. K.: ^{238}U decay series nuclides in the northeastern Arabian Sea: Scavenging rates and cycling processes, Cont. Shelf Res., 14, 251–265, 1994.

Shannon, L. V., Cherry, R. D., and Orren, M. J.: Polonium-210 and lead-210 in the marine environment, Geochim. Cosmochim. Acta, 34, 701–711, 1970.

Shimmield, G. B., Ritchie, G. D., and Fileman, T. W.: The impact of marginal ice zone processes on the distribution of ^{210}Pb, ^{210}Po and ^{234}Th and implications for new production in the Bellingshausen Sea, Antarctica, Deep-Sea Res. II, 42, 1313–1335, 1995.

Stewart, G., Cochran, J. K., Miquel, J. C., Masqué, P., Szloseka, J., Rodriguez y Bana, A. M., Fowler, S. W., Gasser, B., and Hirschberg, D. J.: Comparing POC export from ^{234}Th/^{238}U and ^{210}Po/^{210}Pb disequilibria with estimates from sediment traps in the Northwest Mediterranean, Deep-Sea Res. I, 54, 1549–1570, 2007.

Strickland, J. D. H. and Parsons, T. R.: A Practical Handbook of Seawater Analysis, Fish. Res. Board Can. Bull., 167, 163rd Ed., 311 pp, Queen's Printer, Ottawa., 1984.

Szlosek, J., Cochran, J. K., Miquel, J. C., Masqué, P., Armstrong, R., Fowler, S., Gasser, B., and Hirschberg, D. J.: Particulate organic carbon-^{234}Th relationships in particles separated by settling velocity in the Northwest Mediterranean Sea, Deep-Sea Res. II, 56, 1519–1532, 2009.

Tateda, Y., Carvalho, F. P., Fowler, S. W., and Miquel, J.-C.: Fractionation of ^{210}Po and ^{210}Pb in coastal waters of the Northestern Mediterranean continental margin, Cont. Shelf Res., 23, 295–316, 2003.

Thomson, J. and Turekian, K. K.: ^{210}Po and ^{210}Pb distributions in ocean water profiles from the eastern South Pacific, Earth Planet. Sci. Lett., 32, 297–303, 1976.

Tsai, A.-Y., Gong, G. C., Chiang, K. P., Chao, C.-F., Liao, H.-K., and Shiah, F. K.: Temporal and spatial variations of picoplankton and nanoplankton and short-term variability related to stormy weather in the Danshui River estuary in northern Taiwan, Terr. Atmos. Ocean. Sci., 22, 79–89, 2011.

Tseng, C. M., Wong, G. T. F., Lin, I. I., Wu, C. R., and Liu, K. K.: A unique seasonal pattern in phytoplankton biomass in low-latitude waters in the South China Sea, Geophys. Res. Lett., 32, L08608, doi:10.1029/2004GL022111, 2005.

Turekian, K. K., Nozaki, Y., and Benniger, L.: Geochemistry of atmospheric radon and radon products, Annu. Rev. Earth Planet. Sci., 5, 227–255, 1977.

Verdeny, E., Masqué, P., Maiti, K., Garcia-Orellana, J., Brauch, J. M., Mahaffey, C., and Benitez-Nelson, C. R.: Particle export within cyclonic Hawaiian lee eddies derived from Pb-210-Po-210 disequilibrium, Deep-Sea Res. II, 55, 1461–1472, 2008.

Verdeny, E., Masqué, P., Garcia-Orellana, J., Hanfland, C., Cochran, J. K., and Stewart, G.: POC export from ocean surface waters by means of ^{234}Th/^{238}U and ^{210}Po/^{210}Pb disequilibria: A review of the use of two radiotracer pairs, Deep-Sea Res. II, 56, 1502–1518, doi:10.1016/j.dsr2.2008.12.018, 2009.

Wei, C.-L. and Murray, J. W.: ^{234}Th/^{238}U disequilibria in the Black Sea, Deep-Sea Res., 38, 855–873, 1991.

Wei, C. L. and Murray, J. W.: Temporal variation of ^{234}Th activity in the water column of Dabob Bay: Particle scavenging, Limnol. Oceanogr., 37, 296–314, 1992.

Wei, C.-L. and Murray, J. W.: The behavior of scavenging isotopes in marine anoxic environments: Lead-210 and polonium-210 in the water column of the Black Sea, Geochim. Cosmochim. Acta, 58, 1795–1811, 1994.

Wei, C.-L., Jen, K.-L., and Chu, K.: Sediment trap experiments in the water column off southwestern Taiwan: ^{234}Th fluxes, J. Oceanogr., 50, 403–414, 1994.

Wei, C.-L., Chou, L.-H., Tsai, J.-R., Wen, L.-S., and Pai, S.-C.: Comparative geochemistry of ^{234}Th, ^{210}Pb, and ^{210}Po: A case study in the Hung-Tsai Trough off southwestern Taiwan, Terr. Atmos. Ocean. Sci., 20, 411–423, doi:10.3319/TAO.2008.01.09.01(Oc), 2009.

Wei, C.-L., Chen, P.-R., Lin, S.-Y., Sheu, D. D., Wen, L.-S., and Chou, W.-C.: Distributions of ^{210}Pb and ^{210}Po in surface waters surrounding Taiwan: A synoptic observation, Deep-Sea Res. II, submitted.

Wong, C. S., Whitney, F. A., Crawford, D. W., Iseki, K., Matear, R. J., Johnson, W. K., and Page, J. S.: Seasonal and interannual variability in particle fluxes of carbon, nitrogen and silicon from time series of sediment traps at Ocean Station P, 1982–1993: relationship to changes in subarctic primary productivity, Deep-Sea Res. II, 46, 2735–2760, 1999.

Wong, G. T. F., Ku, T. L., Mulholland, M., Tseng, C. M., and Wang, D. P.: The SouthEast Asian time-series study (SEATS) and the biogeochemistry of the South China Sea - An overview, Deep-Sea Res. II, 54, 1434–1447, doi:10.1016/j.dsr2.2007.05.012, 2007.

Xu, C., Santschi, P. H., Hung, C.-C., Zhang, S., Schwehr, K. A., Roberts, K. A., Guo, L. D., Gong, G.-C., Quigg, A., Long, R. A., Pinckney, J., Duan, S. W., Amon, R., and Wei, C. L.: Controls of Th-234 removal from the oligotrophic ocean by polyuronic acids and modification by microbial activity, Mar. Chem., 123, 111–126, 2011.

Xu, L. Q., Liu, X. D., Sun, L. G., Yana, H., Liu, Y., Luo, Y. H., Huang, J., and Wang, Y. H.: Distribution of radionuclides in the guano sediments of Xisha Islands, South China Sea and its implication, J. Environ. Rad., 101, 362–368, 2010.

Yang, W., Huang, Y., Chen, M., Zhang, L., Li, H., Liu, G., and Qiu, Y.: Disequilibria between ^{210}Po and ^{210}Pb in surface waters of the southern South China Sea and their implications, Science in China: Series D, Earth Sci., 49, 103–112, doi:10.1007/s11430-004-5233-y, 2006.

Yang, W. F., Huang, Y. P., Chen, M., Qiu, Y. S., Peng, A. G., and Lei, Z.: Export and remineralization of POM in the Southern Ocean and the South China Sea estimated from ^{210}Po/^{210}Pb disequilibria, Chinese Sci. Bull., 54, 2118–2123, doi:10.1007/s11434-009-0043-4, 2009.